Assessing the agreement between the pneumatic and the flow-centrifuge method for estimating xylem safety in temperate diffuse-porous tree species

Paligi, S. S.; Link, R. M.; Isasa, E.; Bittencourt, P.; Cabral, J. S.; Jansen, S.; Oliveira, R. S.; Pereira, L.; Schuldt, B.

DOI:
10.1111/plb.13573

plant biology

Plant Biology ISSN 1435-8603

RESEARCH ARTICLE

Assessing the agreement between the pneumatic and the flow-centrifuge method for estimating xylem safety in temperate diffuse-porous tree species

S. S. Paligi[1], R. M. Link[1,2], E. Isasa[1], P. Bittencourt[3], J. S. Cabral[4,5], S. Jansen[6], R. S. Oliveira[7], L. Pereira[6] & B. Schuldt[1,2]

1 Chair of Ecophysiology and Vegetation Ecology, Julius-von-Sachs Institute of Biological Sciences, University of Würzburg, Würzburg, Germany
2 Chair of Forest Botany, Institute of Forest Botany and Forest Zoology, Technische Universität Dresden, Tharandt, Germany
3 College of Life and Environmental Sciences, University of Exeter, Exeter, UK
4 Ecosystem Modeling Group, Center for Computational and Theoretical Biology, University of Würzburg, Würzburg, Germany
5 School of Biosciences, College of Life and Environmental Sciences, University of Birmingham, Birmingham, UK
6 Institute of Botany, Ulm University, Ulm, Germany
7 Department of Plant Biology, Instituto de Biologia, University of Campinas, Campinas, SP, Brazil

Keywords
Drought tolerance traits; flow-centrifuge; method comparison; plant pneumatics; Pneumatron; transport; vulnerability curve; xylem embolism resistance.

Correspondence
R. M. Link and B. Schuldt, Chair of Ecophysiology and Vegetation Ecology, Julius-von-Sachs-Institute of Biological Sciences, University of Würzburg, Julius-von-Sachs-Platz 3, Würzburg 97082, Germany.
E-mail: roman.link@plant-ecology.de (R. M. L.); bernhard.schuldt@plant-ecology.de (B. S.)

Present address
Plant Ecology and Ecosystems Research, Albrecht von Haller Institute for Plant Sciences, University of Goettingen, Göttingen, Germany

S. S. Paligi and R. M. Link contributed equally to this work.

Editor
B. Choat

Received: 16 March 2023;
Accepted: 6 July 2023

doi:10.1111/plb.13573

ABSTRACT

- The increasing frequency of global change-type droughts has created a need for fast, accurate and widely applicable techniques for estimating xylem embolism resistance to improve forecasts of future forest changes.
- We used data from 12 diffuse-porous temperate tree species covering a wide range of xylem safety to compare the pneumatic and flow-centrifuge method, two rapid methods used for constructing xylem vulnerability curves. We evaluated the agreement between parameters estimated with both methods and the sensitivity of pneumatic measurements to the duration of air discharge (AD) measurements.
- There was close agreement between xylem water potentials at 50% air discharged (PAD), estimated with the Pneumatron, and 50% loss of hydraulic conductivity (PLC), estimated with the flow-centrifuge method (mean signed deviation: 0.12 MPa, Pearson correlation: 0.96 after 15 s of gas extraction). However, the relationship between the estimated slopes was more variable, resulting in lower agreement in the xylem water potential at 12% and 88% PAD/PLC. The agreement between the two methods was not affected by species-specific vessel length distributions. All pneumatic parameters were sensitive to AD time. Overall agreement was highest at relatively short AD times, with an optimum at 16 s.
- Our results highlight the value of the Pneumatron as an easy and reliable tool to estimate 50% embolism thresholds for a wide range of diffuse-porous temperate angiosperms. Further, our study provides a set of useful metrics for methodological comparisons of vulnerability curves in terms of systematic and random deviations, as well as overall agreement.

INTRODUCTION

Over the last decades, unprecedented climate fluctuations and the resulting hotter drought events have led to large-scale tree mortality events worldwide (Allen *et al.* 2010, 2015; Brando *et al.* 2019). Such tree mortality events are increasingly likely (Brodribb *et al.* 2020), given the global rise in frequency, intensity and duration of drought spells predicted by current climate projections (*cf.* Field *et al.* 2012; Trenberth *et al.* 2014).

A better understanding of the physiological mechanisms underlying tree mortality is necessary to improve predictions of demographic and compositional changes in forest ecosystems (Allen *et al.* 2010; McDowell *et al.* 2013a, 2013b). This has created increased interest in traits quantifying the vulnerability of xylem to drought-induced embolism (Choat *et al.* 2018; Brodribb *et al.* 2020), usually expressed as the parameters of xylem vulnerability curves (VCs). These curves describe the consecutive loss of hydraulic conductance (percentage loss of conductivity, PLC) with increasingly negative xylem pressures

(*cf.* Sperry *et al.* 1988; Cochard *et al.* 2013). Most commonly, VCs are quantified by the water potentials at 12% (P_{12}), 50% (P_{50}) or 88% (P_{88}) loss of hydraulic conductance and the slope of the curve at one of these points. These parameters have been linked to mechanistic thresholds for xylem functioning (Brodribb & Cochard 2009; Urli *et al.* 2013; Delzon & Cochard 2014), and are closely coordinated with stomatal regulation (Martin-StPaul *et al.* 2017). Across biomes, xylem embolism resistance is associated with the susceptibility of a species to drought-induced mortality (Anderegg *et al.* 2016; Adams *et al.* 2017), which mirrors the distribution of species along aridity gradients (Blackman *et al.* 2014; Trueba *et al.* 2017; Oliveira *et al.* 2019). Because of their direct mechanistic interpretation, VC parameters and derived quantities, such as hydraulic safety margins (Meinzer *et al.* 2009), are increasingly incorporated in process-based vegetation models to describe drought responses and associated drought-induced tree mortality (see Li *et al.* 2022 for a review).

Xylem VCs are measured using a large number of different techniques. These include the bench dehydration (Sperry *et al.* 1988), air injection (Cochard *et al.* 1992), flow-centrifuge (Cochard *et al.* 2005), micro- computed tomography (CT; Brodersen *et al.* 2010), pneumatic (Pereira *et al.* 2016), optical (Brodribb *et al.* 2016) and relative water loss (Rosner *et al.* 2019) methods. However, at least some of these methods are not fully reliable across species with differing wood anatomies; for instance, due to measurement artefacts associated with vessel length (Cochard *et al.* 2013; Jansen *et al.* 2015). Moreover, not all methods are equally suitable for rapid measurements of large numbers of samples (Cochard *et al.* 2013; Nolf *et al.* 2017). For a broader assessment of embolism resistance, the development of methods for the measurement of xylem embolism that are simple, accessible, reliable and applicable to a wide range of taxonomic groups and xylem types is required.

In this work, we test the agreement between two rapid measurement methods for vulnerability curves– the flow-centrifuge method and the pneumatic method. Both methods have the advantage of being able to obtain an entire VC based on a single sample. In the flow-centrifuge method, a branch sample is placed into a custom-built centrifuge rotor and spun at high rotational velocities, for example, in a so-called Cavitron, to generate a negative xylem pressure, while simultaneously measuring conductivity by tracking the rate of water flow through the sample (Cochard *et al.* 2005). This reduces the time for one VC measurement to around 30–60 min. However, there is evidence that the flow-centrifuge method is subject to vessel length-related measurement artefacts and underestimates embolism resistance for long-vesselled species (Li *et al.* 2008; Choat *et al.* 2010; Cochard *et al.* 2010), which limits its applicability to conifers and angiosperms with short vessels, unless longer centrifuge rotors are used (*cf.* Burlett *et al.* 2022). An alternative is the pneumatic method, a novel route for fast measurements of embolism propagation in intact vessels (Pereira *et al.* 2016; Jansen *et al.* 2020). The pneumatic method estimates the amount of xylem embolism by measuring how the air volume in xylem conduits of bench-dried plant samples changes with increasingly negative xylem pressure. With the Pneumatron (Pereira *et al.* 2020a), an automated device is available that can measure air discharge at a high temporal resolution and permits high sample throughput (Jansen *et al.* 2020; Pereira *et al.* 2020a). The pneumatic method has already been used to construct VCs for a wide variety of species of differing origin and wood type (Pereira *et al.* 2016, 2020a; Zhang *et al.* 2018; de V Barros *et al.* 2019; Sergent *et al.* 2020; Wu *et al.* 2020; Brum *et al.* 2023; Zhao *et al.* 2023). As the measurement principle of the Pneumatron does not directly depend on the measurement of xylem water transport, and embolism is induced by bench dehydration, it is assumed to be relatively robust against measurement artefacts related to sample excision and preparation, as well as vessel length-related artefacts (Pereira *et al.* 2016, 2020a). However, while there is good evidence that the method is not sensitive to vessel length (Pereira *et al.* 2021), methodological comparisons show that the pneumatic method does not work for torus-bearing conifer species (Zhang *et al.* 2018; Sergent *et al.* 2020; Zhao *et al.* 2023). Moreover, its estimates are known to be sensitive to the choice of the reservoir volume and the duration of the air discharge measurement (Pereira *et al.* 2016, 2020a; Yang *et al.* 2023).

Over the last decade, considerable attention has been paid to measurement artefacts in methods to quantify embolism resistance. Much less attention has been dedicated to the ways method agreement is quantified, and we still lack a rigorous statistical framework to compare embolism resistance methods. To address this, we define a set of metrics to describe the agreement between VC parameter estimates and entire curves, and use them to compare the pneumatic and flow-centrifuge methods, with special emphasis on the influence of the air discharge (AD) interval on the outcome of the pneumatic method. We further investigate the influence of vessel length on the agreement between the two methods. Based on a dataset of vulnerability curve measurements from 36 trees belonging to 12 temperate, diffuse-porous tree species, we (i) assess how well the parameters of the vulnerability curves obtained with the pneumatic method (Pneumatron) agree with estimates obtained from the flow-centrifuge method (Cavitron) in terms of systematic deviations, random deviations and overall agreement, and (ii) use these agreement metrics to identify the optimal duration for air discharge measurements.

MATERIAL AND METHODS

Plant material

This study is based on plant material from 12 temperate diffuse-porous tree species (Table 1). The samples for pneumatic and hydraulic VCs were collected between mid-July and mid-September 2019 from the nursery in the Stutel-Arboretum of the Bavarian State Institute for Viticulture and Horticulture (LWG) in Veitshöchheim, Germany (49°51′59″ N, 9°51′8″ E). To assess anomalies in the VC data for some of the species (see below), additional branch samples were obtained from adult *Tilia cordata* and *Tilia platyphyllos* trees growing at Ulm University, Germany (48°25′20.3″ N, 9°57′20.2″ E) and of *Tilia japonica* from the Würzburg Botanical Garden, Germany (49°45′56.7″" N 9°55′58.1″ E) in September 2020. The samples for vessel length measurements were collected from the same trees from the Stutel-Arboretum in October 2021. For all measurements, one sun-exposed branch 70–120 cm in length was collected per tree before 09:30 h to ensure sample excision in a relaxed state. Before starting the measurements, the branches were rehydrated in the laboratory for at least 1 h by placing their basal end in water to relax the xylem. Complete rehydration of the samples was assumed when initial water potential values reached *ca.* −0.1 MPa.

Table 1. List of the 12 diffuse-porous tree species studied, average midday leaf water potential (Ψ_{midday}) measured in August 2020, and the average diameter at breast height (DBH) of the selected trees per species (mean ± SE); n_P and n_H indicate the number of xylem vulnerability curves measured for the pneumatic and the flow-centrifuge method, respectively (values in brackets indicate when branch samples were collected from a single tree).

species	family	n_P	n_H	Ψ_{midday} (MPa)	DBH (cm)
Betula pendula	Betulaceae	3	3	−1.60 ± 0.04	10.93 ± 0.64
Betula utilis	Betulaceae	3	3	−1.54 ± 0.06	08.88 ± 0.42
Carpinus betulus	Betulaceae	3	3	−2.47 ± 0.06	10.75 ± 0.44
Crataegus persimilis	Rosaceae	3	3	−3.42 ± 0.18	07.55 ± 0.16
Ostrya carpinifolia	Betulaceae	3	3	−2.97 ± 0.11	09.18 ± 0.11
Platanus x acerifolia	Platanaceae	3	3	−1.74 ± 0.03	10.00 ± 0.24
Platanus orientalis	Platanaceae	3	3	−1.51 ± 0.04	12.07 ± 0.35
Pyrus calleryana	Rosaceae	2	3	−3.52 ± 0.30	11.88 ± 0.32
Sorbus lalifolia	Rosaceae	3	3	−3.64 ± 0.19	09.30 ± 0.39
*Tilia cordata**	Malvaceae	5 (1)	5 (1)	NA	28.00 ± 0.00
Tilia cordata#	Malvaceae	3	3	−1.90 ± 0.04	11.40 ± 0.46
Tilia japonica	Malvaceae	3 (1)	4 (1)	NA	30.40 ± 0.00
*Tilia platyphyllos**	Malvaceae	4 (1)	7 (1)	NA	70.00 ± 0.21
Tilia platyphyllos#	Malvaceae	3	3	−1.80 ± 0.08	12.38 ± 0.21

Asterisks (*) indicate xylem pressures measured with stem psychrometers; hashes (#) indicate individuals from the same species measured with a pressure chamber.

Air discharge measurements with the Pneumatron

Branch xylem vulnerability curves based on the pneumatic method (Pereira *et al.* 2016) were obtained for 44 samples from 35 trees (Table 1) using a Pneumatron device. The reservoir pressure was tracked with the Pneumatron in 0.5 s intervals over a span of 2 min per measurement (including a pump time of approximately 2 s in semi-automated mode and a few milliseconds in automated mode, which was subtracted later for comparability). The amount of air discharged (AD) into the reservoir was calculated based on the ideal gas law according to Pereira *et al.* (2016). The semi-automated mode of the Pneumatron was used to measure AD for the samples obtained from Veitshöchheim and Würzburg, whereas the additional branch samples of *T. cordata* and *T. platyphyllos* processed in Ulm were measured in automated mode. After each AD measurement, the xylem water potential was measured (see below). The maximum detectable amount of AD is associated with a change of pressure in the system by ~ 50 kPa (Pereira *et al.* 2020a). As the time necessary for a pressure change of 50 kPa depends on the ratio between the reservoir volume (including the volume of the air-filled, cut-open conduits) and the volume of gas extracted from intact embolized conduits, the choice of the optimal reservoir volume is crucial (*cf.* Pereira *et al.* 2020a). For this study, reservoir volumes of 1.7–3.3 ml were selected, depending on the species.

To minimize air entry from outside the xylem, potential leakage points of the Pneumatron samples were sealed using a fast-drying contact adhesive (Loctite 431 with Loctite activator SF 7452; Henkel, Düsseldorf, Germany) before each measurement and after unexpected increases in AD. Fruits present on the branches were removed and the remaining scars sealed with the same adhesive, as they easily detach at more negative water potentials, which opens potential pathways for air entry. In the case of *Crataegus persimilis*, thorns were removed and sealed in the same manner to ease handling of the branches. After rehydration, the basal ends of the branches were cleaned with a sharp razor blade to clear obstructions for airflow (Pereira *et al.* 2016; Jansen *et al.* 2020). This cut was intentionally performed in air to ensure the cut-open conduits were fully embolized when starting pneumatic measurements (Pereira *et al.* 2016). The branch was then connected to the pneumatic apparatus using rigid and elastic tubing tightened with plastic clamps (see Figuress S1 and S2). The volume of the elastic tube was kept as small as possible to minimize pressure-dependent changes in reservoir volume.

Between measurements, the branches were dehydrated at room temperature on a laboratory bench to induce embolism (Sperry *et al.* 1988). The drying intervals were initially about 15–30 min and subsequently increased to 1–4 h, depending on how quickly the sample dried. To minimize transpiration and to allow xylem water potential to equilibrate after each drying interval, the samples were bagged in dark plastic bags for 30–60 min between drying intervals, which is safely above the minimum sufficient equilibration time of 10–30 min reported by Rodriguez-Dominguez *et al.* (2022). Pneumatron VCs were constructed simultaneously for multiple branches (Figuress S1–S3). The elastic tubing was always kept attached to the samples when switching branches to maintain the reservoir volume constant throughout measurements. AD measurements were taken until constancy in AD in consecutive measurements over at least 24 h, or until the minimum xylem water potential measurable with the Scholander pressure chamber (−10 MPa) was reached. This resulted in measurement durations of 3–7 days as well as in 10–20 AD and leaf water potential measurements per branch when using the semi-automated mode of the Pneumatron. The percentage of air discharged (PAD) was calculated as described by Pereira *et al.* (2016):

$$PAD_i = 100 \cdot \frac{AD_i - AD_{min}}{AD_{max} - AD_{min}}, \quad (1)$$

where AD_i is the amount of air discharged for measurement i, AD_{min} is the minimum amount of air discharged from the fully hydrated branch, and AD_{max} is the maximum amount of air discharged from the branch when completely desiccated.

Xylem water potential measurement

For the 35 branch samples measured with a Pneumatron in semi-automated mode, the xylem water potential was measured on two excised leaves using a Scholander pressure chamber (PMS Instruments, Corvallis, OR, USA) after every AD measurement. When the petiole was too small for measurement in the pressure chamber, small terminal twigs were used. The cut was immediately sealed with instant adhesive (Loctite 431) to prevent leakage. For the nine branches of *T. cordata* and *T. platyphyllos* measured using the automated mode, a stem psychrometer (ICT International, Armidale, NSW Australia) was installed at the basal part of the branch to record xylem pressures in 15-min intervals. To obtain pressure estimates for each point in time and to reduce the impact of measurement uncertainty in the psychrometric water potentials, the psychrometer measurements for each sample were smoothed with shape-constrained additive models using monotonically decreasing P-splines based on R package scam version 1.2-8 (Pya & Wood 2015).

Measurements of vulnerability curves with the flow-centrifuge method

Vulnerability curve measurements based on the flow-centrifuge technique (Cochard *et al.* 2005) were performed for 49 samples from 36 trees using a Cavitron device built from a Sorval RC 5 series centrifuge with manual control of rotation speed, and using the Cavisoft software (Cavisoft version 5.2.1, University of Bordeaux, Bordeaux, France). The 2019 Cavitron measurements were also used in Isasa *et al.* (2023). Samples were recut several times under water to a final length of 27.5 cm to release the tension in the xylem (Torres-Ruiz *et al.* 2015). Subsequently, the non-flushed branch segments were inserted in a custom-made rotor after removing the bark at both ends. They were then spun using the principle of centrifugal force to generate a negative pressure in the xylem segment while simultaneously measuring hydraulic conductance. Flow centrifuge measurements were performed with filtered (0.2 μm) and degassed demineralized water enriched with 10 mM KCl and 1 mM $CaCl_2$. Measurements began at xylem water potentials of around −0.8 MPa and were continued under increasingly negative xylem pressures until a PLC of at least 90%.

Vessel length measurements

To assess whether differences in VC parameters obtained with the two methods result from vessel length-related measurement artefacts, we estimated vessel lengths on three to four trees of each study species (42 samples in total) with the pneumatic method described by Pereira *et al.* (2020b). The fully rehydrated samples were connected to the Pneumatron with their apical end (diameter 5–6 mm) and successively shortened from the basal end while recording length and associated air discharge rates. The resulting air discharge profiles were used to estimate vessel length distributions using analytical solutions for the expected discharge profile based on Link *et al.* (2018).

Statistical analysis

All data handling and statistical analyses were performed in R version 4.0.2 (R Core Team 2020) in the framework of the tidyverse (Wickham *et al.* 2019). Both the vulnerability curves based on pneumatic and on flow-centrifuge measurements were described with tree-level nonlinear regression models using the logistic function of (Pammenter & Van der Willigen 1998). For the flow-centrifuge method, vulnerability curves were based on the raw conductivity measured from the Cavitron (*cf.* Ogle *et al.* 2009):

$$K_i \sim \text{Normal}\left(k_{\text{sat}} \cdot \left(1 - \frac{1}{1+\exp\left(\frac{S_{50\text{H}}}{25}\left(P_\text{i} - P_{50\text{H}}\right)\right)}\right), \sigma_\text{K}\right), \quad (2)$$

where K_i and P_i are the measured hydraulic conductivity and xylem pressure for observation i, respectively, k_{sat} is the hydraulic conductivity under fully saturated conditions, $P_{50\text{H}}$ is the water potential at 50% loss of conductivity, $S_{50\text{H}}$ is the slope at $P_{50\text{H}}$ and σ_K is the residual standard deviation. For the pneumatic measurements, analogous models were constructed based on PAD for estimating $P_{50\text{P}}$ (Equation 1):

$$\text{PAD}_i \sim \text{Normal}\left(\frac{100}{1+\exp\left(\frac{S_{50\text{P}}}{25}\left(P_\text{i} - P_{50\text{P}}\right)\right)}, \sigma_{\text{PAD}}\right) \quad (3)$$

To evaluate the effect of the air-discharge time on the agreement of the estimates of vulnerability curve parameters, separate pneumatic vulnerability curves were fit on PAD calculated for all measurement durations between the initial pressure immediately after pumping and variable final pressures at 0.5 s intervals, from 4.5 to 115 s. The P_{12} and P_{88} pressures were calculated from the estimated model parameters (P_{50} and S_{50}) as $P_Q = 25 \cdot \ln(100/Q - 1)/S_{50} + P_{50}$. Confidence intervals for P_{12} and P_{88} were based on 10,000 random samples from the model variance–covariance matrix (*cf.* "population prediction intervals" in Lande *et al.* 2003; Bolker 2008). The uncertainty in the estimates of VC parameters was propagated into species-level estimates by inverse-variance weighting (*cf.* Hajek *et al.* 2022).

For the vessel length estimates, we assumed vessel length to follow an Erlang(2) distribution, which results in the following model for the observed gas discharge profile:

$$\text{AD}_i \sim \text{Normal}\left(\text{AD}_{\text{max}}\left(\frac{z_\text{i}}{\mu} + 1\right)\exp\left(-\frac{2z_i}{\mu}\right), \sigma\right), \quad (4)$$

where AD_i is the measured amount of air discharge for observation i, AD_{max} is the maximum amount of air discharged, z_i is the current length of the sample, μ is the average vessel length, and σ is the residual standard deviation. Based on the equations in Table S1.1 in Link *et al.* (2018), we further computed the 95th percentile of vessel length, and the fraction of open vessels spanning over the 27.5 cm rotor length of the Cavitron.

We subsequently calculated a set of metrics that describe the degree of agreement of the Pneumatron- and flow-centrifuge-based VC parameter estimates in terms of systematic deviations (the average differences between measurements), random deviations (the degree scatter of these measurements around these averages), and overall agreement (the sum of systematic and random deviations; see Table 2). For the Pneumatron measurements from *Tilia japonica*, *T. cordata* and *T. platyphyllos*, these calculations were based on tree averages of the flow-centrifuge parameters when replicate measurements were performed per tree (Table 1).

In addition to these metrics, we formally tested the agreement between the Cavitron-based estimates of P_{12}, P_{50}, P_{88} and (natural log-transformed) S_{50} and their Pneumatron-based equivalents for AD intervals of 15, 30, 60, 90 and 115 s in a model-based approach (*cf.* Carstensen 2004). Here, we modelled each estimate y_i for observation i from method j for sample k and species l as draws from a normal distribution, with mean μ_{jkl} and residual standard deviation σ_j.

$$y_i \sim \text{Normal}\left(\mu_{jkl} = \boldsymbol{X}\beta_\mu + u_k + v_l, \sigma_j = \exp(\boldsymbol{X}\beta_\sigma)\right)$$

$$u_\text{k} \sim \text{Normal}(0, \tau_\text{u}), v_l \sim \text{Normal}(0, \tau_l) \quad (5)$$

where μ_{jkl} was expressed as a function of a linear predictor $\boldsymbol{X}\beta_\mu$ and random sample (u_k) and species (v_l) effects, while σ_j was

Table 2. Metrics to quantify the agreement between vulnerability curve estimates with their mathematical definition, use and interpretation.

metric	definition	use	interpretation
Mean signed deviation	$MSD = \frac{1}{n}\sum(\theta_P - \theta_H)$	Systematic deviations between two parameters	Average difference between the two parameter estimates ("additive bias" – not affected by variance in estimates). High values indicate a high average difference between the estimates.
Pearson correlation coefficient	$\rho = \frac{cov(\theta_P, \theta_H)}{SD(\theta_P)\ SD(\theta_H)}$	Random deviations between two parameters	Amount of shared variation in the two sets of measurements (not affected by systematic differences). Values close to one indicate a close linear association.
Root mean square deviation	$RMSD = \sqrt{\frac{1}{n}\sum(\theta_P - \theta_H)^2}$	Overall agreement between two parameters	Total amount of variation in the difference between measurements (both systematic and random deviations). High values indicate low agreement between estimates.
L_2 distance	$L_2 = \left(\int_{-\infty}^{\infty}(PLC_H(P) - PLC_P(P))^2\ dP\right)^{1/2}$	Overall agreement over the entire vulnerability curve	Generalization of RMSD to describe the degree of similarity over the entire curves. Identical curves have an L_2 distance of 0; high values indicate a mismatch between curves (*cf.* Cramér 1928).

θ_P and θ_H: sets of parameter estimates obtained with the pneumatic and the flow-centrifuge method, respectively; SD: standard devation; cov: covariance; $PLC_H(P)$ and $PLC_P(P)$: functions describing the expected percentage loss of conductivity based on the pneumatic/hydraulic measurements in dependence of the water potential P, in this example given by the logistic model of Pammenter & Van der Willigen (1998): $PLC(P_i) = \frac{100}{(1+\exp(S_{50}/25\cdot(P_i - P_{50})))}$ (compare Equations 2 and 3).

expressed as a log-linear function of an analogous predictor $\boldsymbol{X}\beta_\sigma$. The predictor matrix $\boldsymbol{X}$ encoded the effect of the different estimation methods based on treatment contrasts (*i.e.*, using the flow-centrifuge as a baseline and estimating its average difference to the estimates based on different Pneumatron discharge times). This formulation permits us to estimate the average systematic deviations between the methods (differences in β_μ). Analogously, differences in the degree of random deviations of a method around its average (and hence its repeatability) can be estimated *via* β_σ. The model was fit using linear mixed effects models based on R package glmmTMB version 1.0.2.1 (Brooks *et al.* 2017) using maximum likelihood estimation. Model assumptions were checked based on residual diagnostic plots.

RESULTS

Vulnerability curves

In general, there was a good visual agreement in overall shape between the flow-centrifuge and pneumatic vulnerability curves (VCs) for most of the species studied (Fig. 1). The average P_{50H} estimates obtained from the flow-centrifuge method covered a wide range of embolism resistance, ranging from −1.85 MPa for *Platanus* × *acerifolia* to −6.02 MPa for *Crataegus persimilis*. Parameters estimated with the pneumatic method largely fell into the same range (Table S1). The observed midday water potentials were all less negative than the P_{50H}, and less negative than the P_{12H} for all species except *Platanus* × *acerifolia* (Table 1, Table S1), indicating the measured VC parameters were consistent with field observations.

However, the estimates in P_{12P}, P_{50P} and P_{88P} for *T. cordata* and *T. platyphyllos* based on the pneumatic method were, on average, at least 0.5 MPa higher than the corresponding estimates of the flow-centrifuge method when their xylem pressure was measured using a pressure chamber (Table S1). As we assumed these differences resulted from inaccurate xylem water potential measurements obtained with the pressure chamber, the subsequent results for these species are based only on the psychrometer-based observations. Additional measurements performed to explain this discrepancy showed that the difference to the flow-centrifuge based curves largely disappeared when xylem pressure was determined by stem psychrometers (with the exception of P_{88P} for *T. cordata*; Table S1; Figure S4).

Agreement between methods

The parameters of the vulnerability curves estimated with the two methods were generally highly correlated, with Pearson correlations above 0.54 for all parameters, and over 0.74 for P_{12}, P_{50} and P_{88} for all AD times considered and all 12 tree species (Table S2). In particular, this was true for the P_{50} estimates, where correlations exceeded 0.95 in all cases. Moreover, the P_{50} estimates of the two methods were very close to the 1:1 line (*cf.* Fig. 2b, Table S2). The Pneumatron-based estimates of the slope of the vulnerability curve, however, showed on average a negative systematic deviation, which ranged from −25.5% (retransformed from log scale, 15 s AD time) to −28.1% (115 s AD time; *cf.* Figs 1 and 2d; Table S2). The deviation was larger in samples with lower slopes (Fig. 2). Due to the direct relationship between slope and P_{50}, the systematically lower slope estimates translated to a less negative P_{12P} (by up to 0.77 MPa on average at 115 s AD time) and, in some cases, a more negative P_{88P} (by up to −0.26 MPa on average at 15 s AD time; Fig. 2, Table S2). For P_{50}, the RMSD (a measure of overall agreement) was between 0.52 and 0.54 MPa for all considered AD times (Table S2).

Influence of discharge time

The pneumatic estimates of all VC parameters were sensitive to the chosen discharge time (Figs 3 and 4). However, the change in agreement with air discharge time was neither consistent between parameters nor between species (Figs 3 and 4, Table S2). Consequently, there were major differences between species in the AD interval at which the lowest deviation between flow-centrifuge and pneumatic estimates of P_{50} (Fig. 3) occurred. Deviation increased with discharge time for

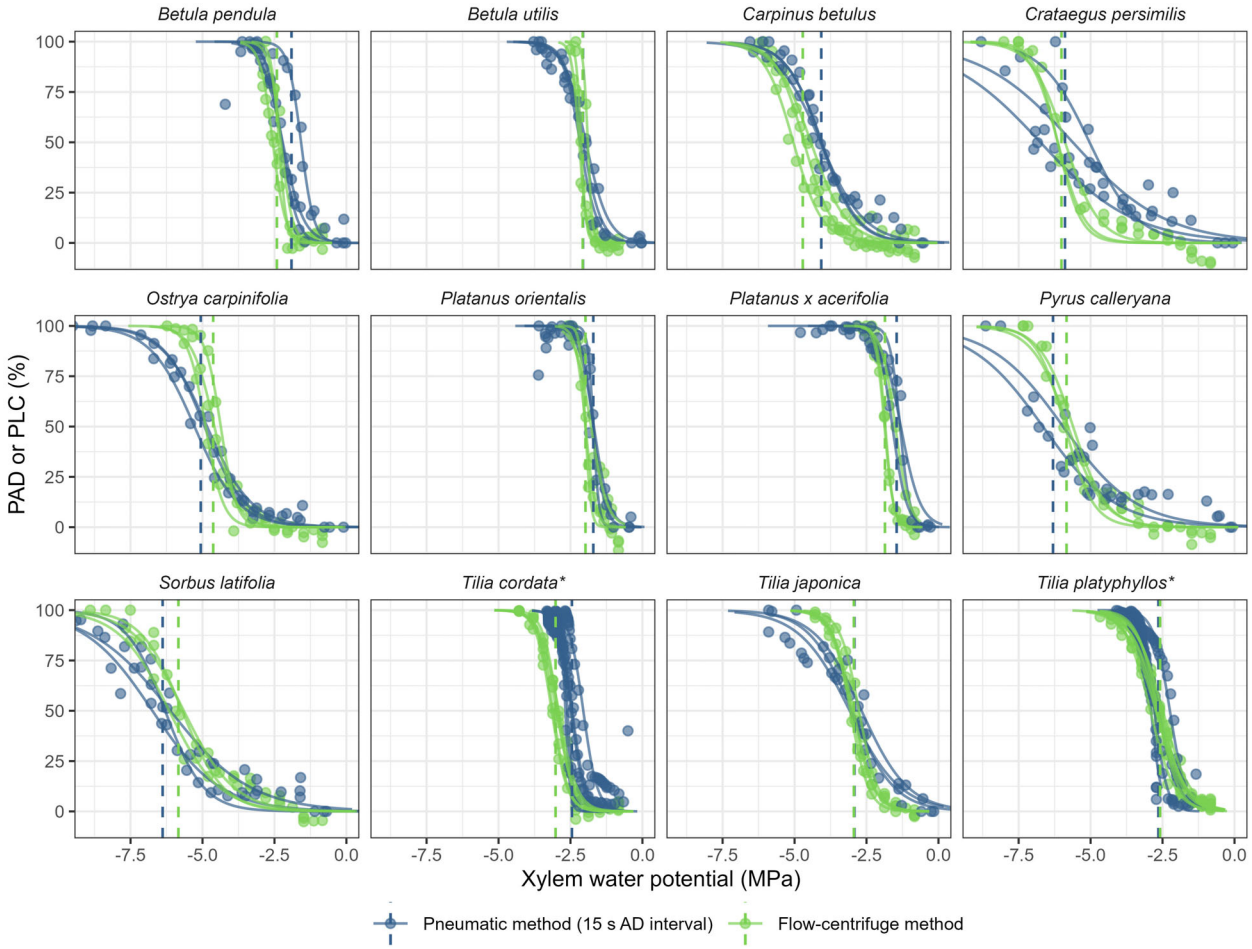

Fig. 1. Xylem vulnerability curves obtained with the pneumatic method after a measurement duration of 15 s (green) and the flow-centrifuge method (blue) for 12 diffuse-porous tree species. Circles: observed values (for centrifuge data, rescaled from conductance to PLC using the estimated k_{sat}); solid lines: predicted PLC/PAD; dashed lines: estimated P_{50}. Asterisks (*) at the end of species names indicate xylem pressure measurements with stem psychrometers.

some species (*Betula pendula*, *B. utilis*, *Crataegus persimilis*, *T. japonica*, and *T. platyphyllos*) and decreased for others (*Ostrya carpinifolia*, *P. orientalis*, *P.* × *acerifolia*, *Pyrus calleryana*, and *Sorbus latifolia*). After accounting for random variation between species and trees, significant systematic differences between the methods remained for all VC parameters at all analysed AD times, except for P_{50} at shorter measurement intervals (Table 3). In addition, the pneumatic method had a significantly lower repeatability (significantly higher random deviations) for all parameters at long AD times (Table 3).

The response of the pneumatic estimates of the VC parameters to AD time was not consistent between parameters (Fig. 4). Depending on the parameter, the overall agreement with the flow-centrifuge method was either highest at short AD times (P_{12}), remained relatively stable over a wide range of AD times (P_{50}, S_{50}) or increased continuously with increasing AD time (P_{88}; Fig. 4, Table 3). The L_2 distance, which describes the overall match of the vulnerability curves over their entire range instead of focusing on a point estimate, reached a minimum at 16 s, although with a relatively broad range of very similar values (Fig. 5). This indicates that the lowest degree of dissimilarity between the curves corresponded to the AD times associated with the lowest systematic differences in P_{50} estimates (Table 3, Table S2; Fig. 4).

Vessel length estimates

The estimated vessel length distributions for the species studied are shown in Fig. 6. The overall mean vessel length was below 11 cm for all species, and below 5 cm when excluding the two *Platanus* species. In addition, the average 95% percentile of vessel length did not exceed the Cavitron rotor length for any of the species studied, although the length of a small fraction of vessels exceeded the rotor length for two species, with on average 2.6% of the vessels exceeding rotor length for *P. orientalis* and 3.1% for *P.* × *acerifolia*. However, there was no significant relationship between the fraction of open vessels over the rotor length and systematic deviations in P_{50} (Figure S5) or in any other VC parameter.

DISCUSSION

Our results suggest a good agreement between P_{50} estimates obtained with the pneumatic method and the flow-centrifuge

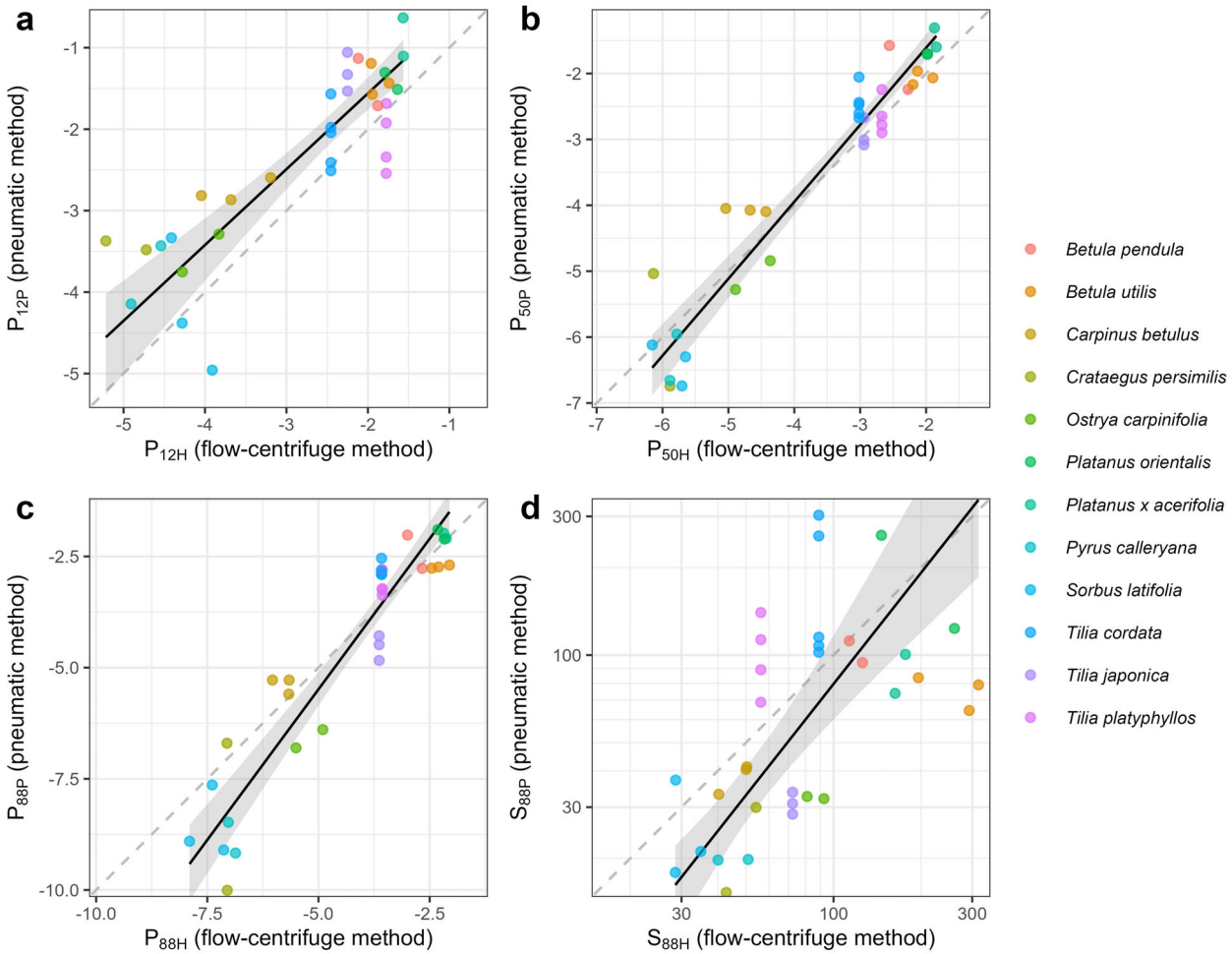

Fig. 2. Relationship between estimates from the flow-centrifuge method (*x*-axis) and the pneumatic method with 15 s air discharge interval (*y*-axis). a: P_{12}, b: P_{50}, c: P_{88} (xylem water potentials at 12%, 50% and 88%, respectively), and d: slope at 50% loss of conductivity (displayed on a log scale). Species identity (empty circles indicate pressure chamber-based *Tilia* measurements); solid black line – standardized major axis (SMA) regression fit through all points ± 95% bootstrap confidence interval; grey dashed line: 1:1 line.

method for constructing vulnerability curves. However, there were higher random and systematic deviations in the slope, P_{12} and P_{88} estimates. The overall agreement between curves depended on the air discharge time for the Pneumatron measurements, as had been predicted based on the unit pipe pneumatic model (Yang *et al.* 2023), with the lowest mismatch found at relatively short measurement durations of around 16 s. Moreover, our vessel length estimates indicate that a vessel length-related bias in the flow-centrifuge measurements can be ruled out as an explanation for the observed differences between methods.

Agreement between flow-centrifuge and pneumatic vulnerability curves

The agreement in P_{50} between the Cavitron and Pneumatron estimates found in our study is in line with results found in similar methodological comparisons involving the pneumatic method (Pereira *et al.* 2016, 2020a; Zhang *et al.* 2018; Sergent *et al.* 2020; Zhao *et al.* 2023; Brum *et al.* 2023; but see also Chen *et al.* 2021). However, we find evidence for high variance and systematic differences in the estimates of the slope of the VC (Fig. 1), which were on average at least 25.5% (15 s air discharge time, *cf.* Table S2) lower for the pneumatic method. Moreover, this difference also resulted in lower agreement in the estimates of P_{12P} and P_{88P}. Similar conclusions were found based on experimental evidence by comparing the pneumatic to the optical method (Pereira *et al.* 2020a; Guan *et al.* 2021), and to a pneumatic modelling approach (Yang *et al.* 2023). While hydraulic measurements are generally not artefact-free (De Baerdemaeker *et al.* 2019), a potential mechanistic explanation for the difference in P_{12} and P_{88} values could be the presence of gas under atmospheric pressure in the cut-open vessel lumina of the Pneumatron stem samples. It has been shown that embolism spreading from these cut-open vessels to interconnected, intact vessels can be enhanced by the proximity to atmospheric gas in the cut-open conduits (Guan *et al.* 2021). A second explanation for the discrepancy observed is that both methods induce negative pressure in different ways, which affects the time to achieve embolism propagation, and thus the overall embolism resistance. While samples in the pneumatic method follow a slow bench dehydration process

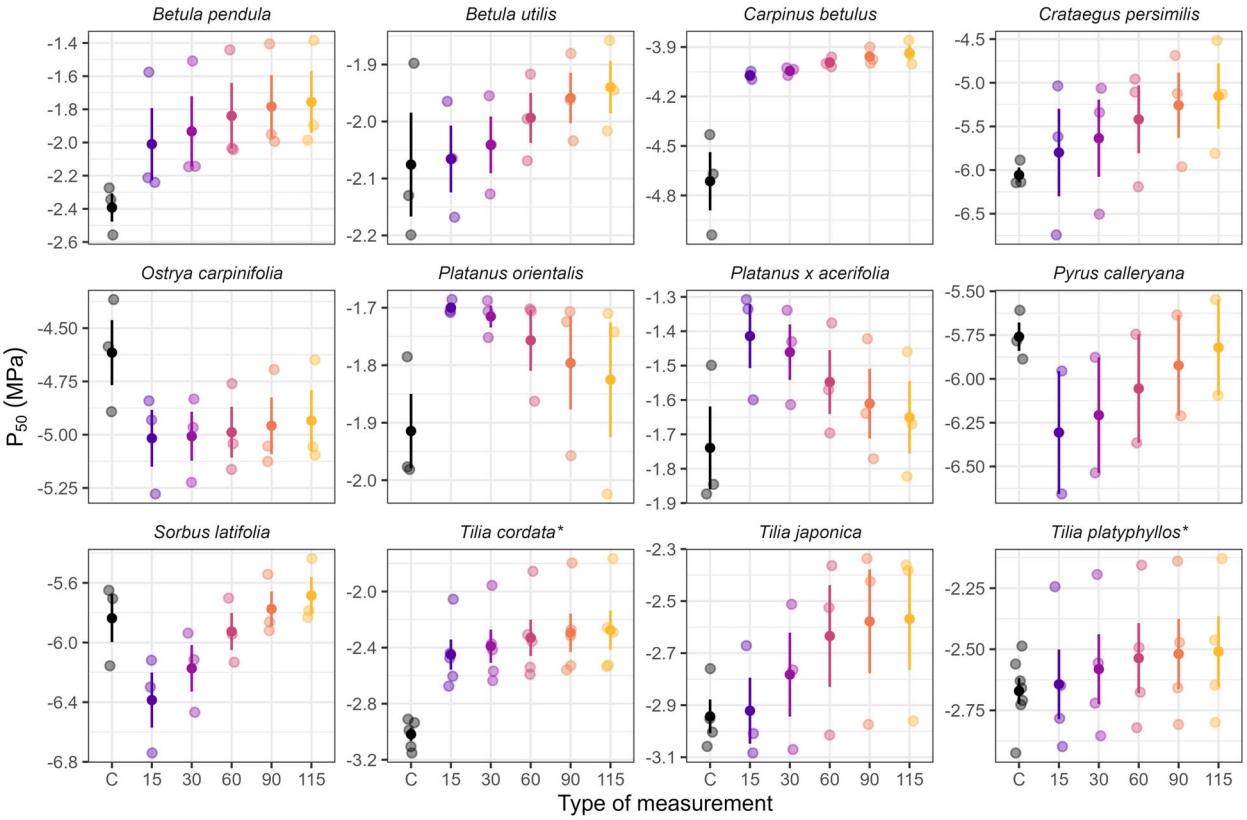

Fig. 3. Comparison of P_{50} values between the flow-centrifuge and different air discharge intervals for the pneumatic method (compared on the same branch). C indicates the P_{50} values from the flow-centrifuge method (black), while 15, 30, 60, 90, and 115 indicate Pneumatron-based estimates with AD measurement intervals from 15 to 115 s (coloured). Shown are the raw estimates overlaid with their mean ± SE. Asterisks (*) at the end of species name indicate xylem pressure was determined using stem psychrometer.

over many hours to a few days, the same embolism propagation in a centrifuge is assumed to occur over a short spinning time of minutes, which may overestimate embolism resistance.

From a theoretical point of view, the gradual loss of conductance and the accompanying increase in the amount of gas in the xylem that occurs when a plant dries (quantified by the PLC and PAD, respectively) are almost certainly positively associated, as during progressive dehydration, they both change monotonously from 0% to 100% over the same range of water potentials. However, as PAD quantifies the gas *volume* inside intact (non-cut open), embolized vessels, while PLC measures the effect of embolism on *conductance*, both can be expected to scale with different powers of vessel dimensions (*cf.* Pereira *et al.* 2016). For a vessel of a given length, the volume scales with the square of its diameter, while its conductivity according to the Hagen-Poiseuille law scales with the fourth power of diameter. Due to these different scaling relationships, the relationship between PAD and PLC is unlikely to be linear. This may induce systematic differences between the parameters of vulnerability curves obtained with different methods, even without any measurement artefact. Specifically, if wider vessels were more vulnerable (*cf.* Isasa *et al.* 2023), this would lead to a steeper increase in PLC per vessel in the less negative pressure range compared to the increase in PAD, which can result in a reduced slope (and potentially a more negative P_{50} estimate) in a volume-based VC compared to a conductance-based VC.

An additional attenuation of the slope of pneumatic VCs can result from treating the unknown true minimum and maximum amount of air discharged (AD_{min} and AD_{max}, *cf.* Equation 1) as fixed quantities measured without error. For hydraulic vulnerability curves, problems induced by treating maximum conductivity as fixed can be circumvented by treating the saturated hydraulic conductivity as an additional model parameter (k_{sat} in Equation 2; *cf.* Ogle *et al.* 2009). Implementing a similar solution for the pneumatic method is not straightforward, as treating both the lower and upper bound as model parameters in sigmoidal models often leads to identifiability issues.

Given the direct mathematical relation between the model parameters, a systematic deviation in the slope will also shift P_{12} and/or P_{88}. This may be problematic, for example, in studies that examine the coordination between stomatal closure and the onset of embolism formation (*cf.* Martin-StPaul *et al.* 2017) or use P_{88} as a proxy for critical desiccation thresholds (*cf.* Blackman *et al.* 2019). Our results indicate that, while the P_{50} estimates of diffuse-porous tree species are relatively consistent between the two methods, the curves obtained may not always be interchangeable.

Effect of the air discharge interval on the agreement between measurements

The optimal air discharge time of 16 s identified in our study is at the lower end of the values typically used in earlier

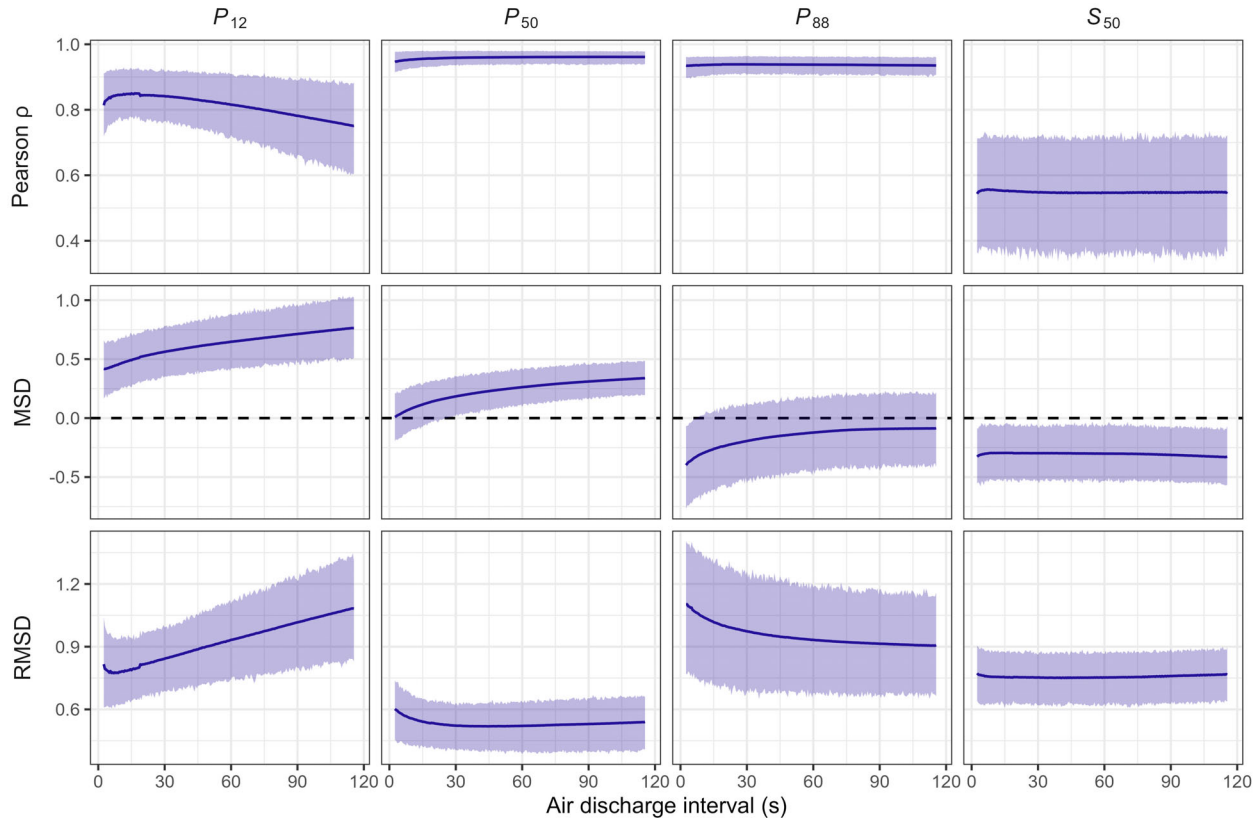

Fig. 4. Statistics describing agreement between the estimated vulnerability curve parameters from the pneumatic method and the flow-centrifuge method *versus* the duration of air discharge measurement (estimates ±95% bootstrap confidence intervals based on 1,000 bootstrap draws). The metrics shown are the Pearson correlation (Pearson ρ) as a measure of random deviation between the two methods (values close to 1 indicate a perfect linear relationship), mean signed deviation (MSD) as a measure of systematic deviations (values close to zero indicate low systematic deviations), and root mean square deviation (RMSD) as a measure of overall agreement (low values indicate a high agreement between methods).

pneumatic studies, ranging from 150 s (Pereira *et al.* 2016; Chen *et al.* 2021), over 120 s (Zhang *et al.* 2018; Sergent *et al.* 2020; Wu *et al.* 2020), to only 30 s (Pereira *et al.* 2020a). However, both the observed sensitivity of the method to AD time and the optimal value at short AD times are consistent with simulation results from the unit pipe pneumatic model, which predicts an optimal time of 15 s or even lower (Yang *et al.* 2023). According to this model, gas extraction times should be relatively short because gas movement from intact, embolized vessels to cut-open vessels is relatively fast across axially interconnected vessels, while diffusion of gas dissolved in conductive vessels is much slower (Yang *et al.* 2023). Indeed, gas diffusion *via* intervessel pit membranes is typically *ca.* 100 times faster than gas diffusion across secondary walls (Sorz & Hietz 2006; Wang *et al.* 2015). On the other hand, while the amount of gas extracted from the aqueous phase increases proportionally over time, it was found to contribute only 9% to the total AD after 15 s of simulation (Yang *et al.* 2023). In addition, although modelling suggests a low influence of radial gas transport (Yang *et al.* 2023), the effect of leakage from potential air entry points outside the xylem will accumulate over time, as the pressure differential over the sample will equilibrate rapidly while the influx from the outside will continue until the sample has reached ambient pressure. Our results illustrate that gains in accuracy due to integrating the change in AD over a larger time interval are overcompensated by an increasing influence from dissolved gas and, potentially, leaks. The higher agreement between methods at lower AD times observed here contrasts with the higher accuracy for longer AD times reported in earlier works using the manual pneumatic method (*cf.* Figure S3 in Pereira *et al.* 2016). This difference likely results from the higher temporal resolution and more accurate AD time measurement possible with the Pneumatron.

To understand how the AD interval can affect the shape of the resulting vulnerability curves, it is helpful to analyse the conditions that would have to be met to ensure AD time does *not* have an effect. A central assumption of the pneumatic method is that the amount of air discharged into the vacuum reservoir over a given time span is a function of the amount of air inside embolized conduits (Jansen *et al.* 2020; Yang *et al.* 2023). To further guarantee that different AD times result in identical vulnerability curves, it is necessary to assume that the shape of the relationship between AD volume and duration of the gas extraction at different dehydration steps is identical up to a constant that is proportional to the total air volume in embolized conduits. However, during the drying process, the xylem undergoes substantial changes that may affect the rate of change in AD over time, such as a change in gas conductivity depending on the number of embolized vessels axially connected. This indicates that the second assumption is likely only

Table 3. Parameter estimates of the linear mixed effect models for the xylem water potential at 12%, 50% and 88% loss of conductivity (P_{12}, P_{50} and P_{88}, respectively) and the natural log-transformed slope at 50% loss of conductivity (S_{50}).

		fixed effects			variance covariates			random effects			
Resp.	Par.	Est.	2.5%	97.5%	Est.	2.5%	97.5%	Par.	Est.	2.5%	97.5%
P_{12}	Hydr.	−2.947	−3.622	−2.266	−3.724	−4.388	−2.890	Samp. SD	0.729	0.430	0.669
	Δ 15 s	0.642	0.344	0.941	1.292	0.315	2.172	Spec. SD	1.025	0.717	1.694
	Δ 30 s	0.730	0.438	1.024	*0.840*	*−0.117*	*1.701*				
	Δ 60 s	0.830	0.536	1.124	*0.919*	*−0.031*	*1.769*				
	Δ 90 s	0.900	0.601	1.200	1.387	0.424	2.251				
	Δ 115 s	0.957	0.651	1.262	1.719	0.756	2.581				
P_{50}	Hydr.	−3.635	−4.625	−2.644	−4.180	−4.830	−3.383	Samp. SD	0.535	0.229	0.363
	Δ 15 s	*0.073*	*−0.099*	*0.245*	1.247	0.312	2.100	Spec. SD	1.266	1.119	2.546
	Δ 30 s	*0.143*	*−0.024*	*0.308*	*0.767*	*−0.161*	*1.615*				
	Δ 60 s	0.218	0.053	0.382	*0.594*	*−0.315*	*1.419*				
	Δ 90 s	0.264	0.096	0.431	*0.868*	*−0.054*	*1.709*				
	Δ 115 s	0.291	0.120	0.461	1.140	0.213	1.986				
P_{88}	Hydr.	−4.335	−5.681	−2.986	−3.953	−4.612	−3.129	Samp. SD	0.769	0.485	0.738
	Δ 15 s	−0.497	−0.818	−0.178	*0.930*	*−0.049*	*1.815*	Spec. SD	1.471	1.505	3.446
	Δ 30 s	−0.446	−0.764	−0.129	*0.543*	*−0.409*	*1.404*				
	Δ 60 s	−0.394	−0.714	−0.076	*0.775*	*−0.158*	*1.611*				
	Δ 90 s	−0.373	−0.695	−0.052	1.095	0.155	1.941				
	Δ 115 s	−0.376	−0.699	−0.053	1.261	0.319	2.106				
$\ln(S_{50})$	Hydr.	4.437	4.055	4.820	−4.583	−5.246	−3.752	Samp. SD	0.582	0.275	0.427
	Δ 15 s	−0.508	−0.706	−0.310	1.817	0.869	2.665	Spec. SD	0.764	0.395	0.947
	Δ 30 s	−0.521	−0.718	−0.324	1.739	0.800	2.577				
	Δ 60 s	−0.541	−0.740	−0.343	1.840	0.905	2.672				
	Δ 90 s	−0.558	−0.760	−0.357	2.020	1.084	2.854				
	Δ 115 s	−0.581	−0.784	−0.378	2.115	1.179	2.950				

Estimates and 95% profile-likelihood based confidence intervals for the flow-centrifuge baseline values (Hydr.) and the deviations from that baseline for different discharge times measured with the Pneumatron (Δ15–Δ115 s) for the fixed effects (limits of agreement) and variance covariate model (differences in measurement variance) as well as the standard deviations of the sample- and species-specific random effects. Values in italics indicate differences that are not significant at 95% level.

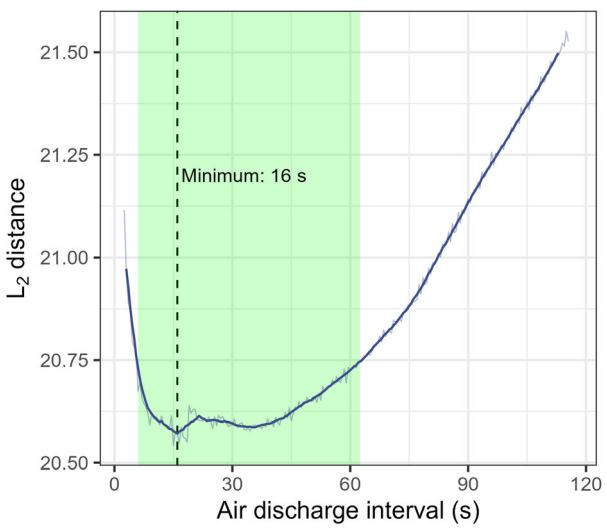

Fig. 5. Average L_2 distance between the pneumatic and flow-centrifuge vulnerability curves *versus* air discharge time as a measure of overall agreement (raw averages and ± 5 s running average). Vertical lines indicate minimum of the running average at 16 s; shaded area indicates the range with a running average differing from the minimum by <1% (6.0–62.5 s).

approximately met under typical measurement conditions. Moreover, it is possible that air-filled spaces that were disconnected from the cut surface at earlier drying steps subsequently become connected to the network of open vessels connecting to the vacuum reservoir (Pereira *et al.* 2016). In such cases, the amount of air in these spaces would not be included in earlier AD estimates, which indicates that the first assumption may not always be met. For these reasons, the relationship between the AD measured after a certain discharge interval and the total amount of air within the xylem is likely empirical. This may explain the pronounced species differences in the response to AD time (Table S2, Fig. 3), and contribute to the previously reported differences in method agreement for species with different types of wood anatomy (Zhang *et al.* 2018). For the reasons discussed above, this variability between species will likely be more pronounced at longer AD times. The choice of short AD times is therefore a simple and pragmatic way to improve the measurement accuracy of pneumatic VCs with automated Pneumatron devices.

Species-specific drying behaviour

As noted previously (Zhang *et al.* 2018; Sergent *et al.* 2020), the agreement between VCs measured with the pneumatic method

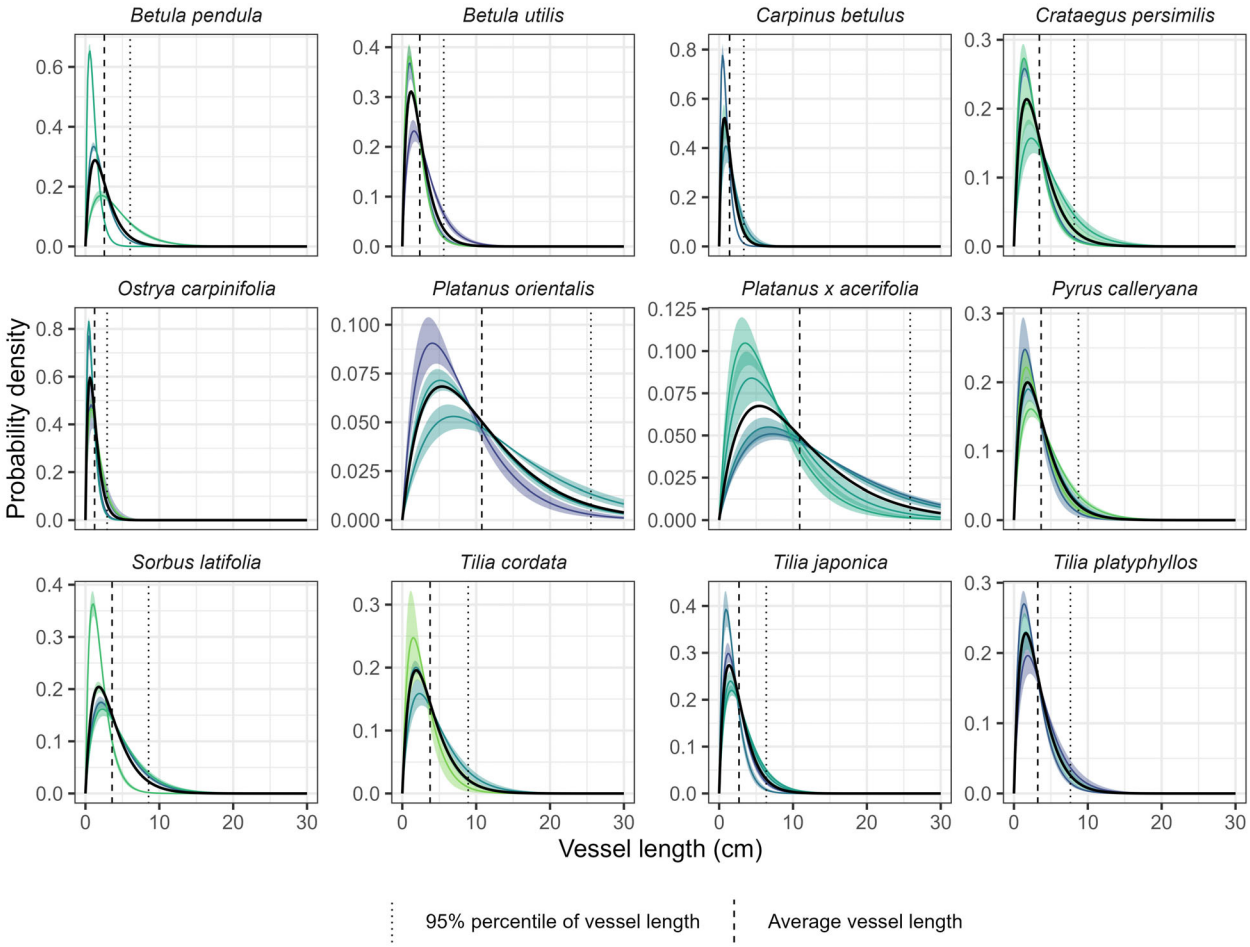

Fig. 6. Estimated vessel length distributions. Coloured lines: probability density functions of individual samples with their 95% CIs; solid black lines: average vessel length distribution; dotted lines: 95th percentile of average vessel length distribution; dashed lines: expected value of average vessel length distribution.

and hydraulic reference methods differs between species. This species specificity is also visible in our results. Importantly, while we find that on average there is a low systematic deviation in P_{50} estimates between the methods, there is a considerable variability between species, independent of AD time. Hence, our results do not rule out pronounced differences in estimated P_{50} for measurements on a particular species, which cannot be attributed with certainty to either of the two methods. However, it is important to consider the different ways water potential is induced and measured in both methods. In this study, we observed a mismatch for *T. cordata* and *T. platyphyllos* when xylem water potential was approximated by leaf water potentials measured with a pressure chamber. This difference largely disappeared when a stem psychrometer was used to determine xylem pressure, indicating that the differences are induced by the water potential measurements. A possible explanation is the presence of mucilage in the xylem tissues of *Tilia* species (Franz & Kram 1985; Pigott 2012), which may affect xylem pressures measured with the pressure chamber technique (Rodriguez-Dominguez *et al.* 2022).

A further explanation for the observed differences between the two *Tilia* species is premature termination of measurements (Brum *et al.* 2023). The truncated shape of the pressure chamber-based Pneumatron VCs for the *Tilia* species (especially *T. cordata*, *cf.* Figure S4), as well as the fact they never reached water potentials substantially more negative than −3 MPa, may indicate that the measurements were terminated before the samples were fully dehydrated. This underestimates AD_{max}, which shifts the curve towards less negative water potentials (Brum *et al.* 2023). As detailed earlier, desiccation was continued until near constancy in AD values over at least 24 h. This criterion to finish AD measurements may not be ideal, as drying may slow down considerably after full stomatal closure, which, especially for isohydric species, may occur in a relatively well-hydrated state. Notably, while *Tilia* species have often been considered to be relatively anisohydric (*cf.* Moser *et al.* 2016; Gillner *et al.* 2017; Kiorapostolou *et al.* 2018), recent work by Leuschner *et al.* (2019) indicates that at least *T. cordata* has a fairly stringent, more isohydric stomatal control mechanism. Given the stronger hydraulic segmentation between leaf petioles and stem xylem anticipated in drought-avoiding and more isohydric species (Hartmann *et al.* 2021), this may have contributed to the mismatch between flow-centrifuge and pneumatic VCs. It is well documented that certain species rely on early leaf shedding as a drought response strategy (Wolfe *et al.* 2016; Hochberg *et al.* 2017), most likely enabled by a pronounced hydraulic segmentation

(*cf*. Pivovaroff *et al*. 2014; Zhu *et al*. 2016; Klepsch *et al*. 2018). As these processes decouple leaf and branch water potentials, measuring leaf water potential with a Scholander pressure chamber may result in extreme water potential readings that do not reflect the actual status in the xylem. Conversely, the slowdown of dehydration induced by leaf shedding may result in prematurely terminated measurements when measuring branch water potentials with a stem psychrometer, or when assuming full dehydration based on the state of the leaves. As a cautionary example, the leaves of *C. persimilis* were almost fully dehydrated on the third day of measurements, while the branch water potential values continued to decline for 7 days. Similar behaviour was reported by Wolfe *et al*. (2016) for the tropical species *Genipa americana*.

Because of these species-specific differences in drying behaviour, the stability of AD_{max} can have a strong influence on the shape of the vulnerability curves as all pneumatic PAD values are normalized against AD_{min} and AD_{max} (*cf*. Brum *et al*. 2023). It may therefore be advantageous to continue the drying process until the constancy of AD_{max} has been confirmed based on several measurements to avoid bias resulting from underestimating AD_{max}. Notably, an important implication of these problems with water potential measurements is that the same bias in water potential may also affect hydraulic VC measurements in other methods that rely on bench dehydration.

Implications for future vulnerability curve method comparisons

An important limitation that affects all VC method comparisons – as well as many other methodological comparisons in biology – is the lack of true reference values. In this study, we used the flow-centrifuge method to obtain reference values for the estimated VC parameters. However, there are many indications that this method is affected by measurement artefacts that arise during sample excision (Wheeler *et al*. 2013) and preparation (Torres-Ruiz *et al*. 2015), or as a result of vessel lengths exceeding the sample dimensions (Choat *et al*. 2010; Martin-StPaul *et al*. 2014; Torres-Ruiz *et al*. 2014). While our vessel length data suggest no length-related bias in the species studied, it is important to point out that a mismatch between curves obtained with the pneumatic method and the flow-centrifuge can result from inaccuracies of either method. While there is rarely a way to overcome the limitation of imperfect reference values, we argue that methodological comparisons of VC methods may benefit from adopting a more principled approach of quantifying the agreement between methods. To our knowledge, none of the previously published VC method comparisons (Li *et al*. 2008; Choat *et al*. 2010; Hacke *et al*. 2015; Brodribb *et al*. 2017; López *et al*. 2019; Venturas *et al*. 2019; Pratt *et al*. 2020; Sergent *et al*. 2020; Zhao *et al*. 2020; Chen *et al*. 2021) differentiate between systematic and random differences in parameter estimates, and neither do they provide metrics that quantify the similarity over the entire curves. This is problematic, as high correlations between methods do not imply the absence of systematic differences (*cf*. Bland & Altman 1986), while average differences alone do not contain information about the strength of the relationship. Explicitly separating different components of method agreement, for instance, with the metrics in Table 2, allows us to more clearly identify how – and why – methods differ. Our study shows that this information can be used to identify optimal AD intervals to maximize agreement in specific parameters or over the entire curve, or to assess whether vessel lengths exceeding the Cavitron rotor size result in stronger deviations from the Pneumatron-based measurements. Model-based approaches, as in Equation 5, moreover, allow formal tests of systematic deviations or differences in repeatability between methods (*cf*. Carstensen 2004).

CONCLUSIONS

The high agreement between the P_{50} estimates with the pneumatic and flow-centrifuge methods indicates that for studies focusing on P_{50} as a proxy of xylem embolism resistance, the Pneumatron provides a valid approach, particularly if short gas discharge times are considered. However, the systematic deviations in VC slope illustrate that the two methods measure different (albeit closely related) processes, which can have important implications for the use and interpretation of parameter estimates, especially in mechanistic models of plant water relations.

Our study further provides new tools for method comparisons when comparing VC methods. Separating overall agreement into systematic deviations (quantifying bias with respect to a reference method) and random deviations (quantifying the repeatability of measurements) allows for more well-informed decisions about the equivalence of different measurement methods, and can be used to decide on best measurement practices, such as the choice of optimal AD intervals.

ACKNOWLEDGEMENTS

We thank Klaus Körber and Andreas Lösch from the Bavarian State Institute for Viticulture and Horticulture (Bayerische Landesanstalt für Wein- und Gartenbau, LWG) for granting access to their research facility at Stutel, and Xinyi Guan for her support with the automated pneumatic measurements. P.R.L.B. acknowledges the Royal Society's Newton International for a Fellowship (NF170370). R.S.O acknowledges CNPq for a productivity grant. S.J. acknowledges funding from the German Research Foundation (Deutsche Forschungsgemeinschaft, DFG, project nr. 457287575). We wish to thank Brendan Choat, Andrew Davis, Laurent Lamarque and three anonymous reviewers for their helpful feedback on the manuscript. Open Access funding enabled and organized by Projekt DEAL.

AUTHOR CONTRIBUTIONS

B. Schuldt and R. M. Link designed the study, S. S. Paligi performed the vessel length distribution and semi-automated pneumatic measurements, technically supported by P. Bittencourt and L. Pereira. L. Pereira conducted the automated pneumatic measurements and E. Isasa the hydraulic measurements. S. S. Paligi and R. M. Link analysed the data. S. S. Paligi, R. M. Link and B. Schuldt wrote the first draft manuscript, which was intensively discussed and revised by all authors.

SUPPORTING INFORMATION

Additional supporting information may be found online in the Supporting Information section at the end of the article.

Table S1. Comparison of the estimated xylem water potential at 12%, 50% and 88% loss of conductivity/percent air discharged (P_{12}, P_{50} and P_{88}, respectively) and slope of the vulnerability curve (S_{50}) for the 12 studied diffuse-porous tree species for the pneumatic (15 s AD interval) and flow-centrifuge method.

Table S2. Summary of a set of metrics describing the agreement between the two analysed methods for the estimated parameters for the xylem water potential at 12%, 50% and 88% loss of conductivity (P_{12}, P_{50} and P_{88}, respectively), and the slope at 50% loss of conductivity (S_{50}).

Figure S1. Documentation of the applied set-up.

Figure S2. Documentation of the stopcock, plastic clamps, and elastic tubing used for connecting the pneumatic apparatus with rigid tubing to the branch.

Figure S3. Storage of branch samples during the measurement.

Figure S4. Comparison of VC and P_{50} estimates measured using stem psychrometer and pressure chamber.

Figure S5. Systematic deviation between pneumatic and hydraulic P_{50} after 15 s AD time vs. the average fraction of open vessels over the rotor length.

REFERENCES

Adams H.D., Zeppel M.J.B., Anderegg W.R.L., Hartmann H., Landhäusser S.M., Tissue D.T., Huxman T.E., Hudson P.J., Franz T.E., Allen C.D., Anderegg L.D.L., Barron-Gafford G.A., Beerling D.J., Breshears D.D., Brodribb T.J., Bugmann H., Cobb R.C., Collins A.D., Dickman L.T., Duan H., Ewers B.E., Galiano L., Galvez D.A., Garcia-Forner N., Gaylord M.L., Germino M.J., Gessler A., Hacke U.G., Hakamada R., Hector A., Jenkins M.W., Kane J.M., Kolb T.E., Law D.J., Lewis J.D., Limousin J.-M., Love D.M., Macalady A.K., Martínez-Vilalta J., Mencuccini M., Mitchell P.J., Muss J.D., O'Brien M.J., O'Grady A.P., Pangle R.E., Pinkard E.A., Piper F.I., Plaut J.A., Pockman W.T., Quirk J., Reinhardt K., Ripullone F., Ryan M.G., Sala A., Sevanto S., Sperry J.S., Vargas R., Vennetier M., Way D.A., Xu C., Yepez E.A., McDowell N.G. (2017) A multi-species synthesis of physiological mechanisms in drought-induced tree mortality. *Nature Ecology & Evolution*, **1**, 1285–1291.

Allen C.D., Breshears D.D., McDowell N.G. (2015) On underestimation of global vulnerability to tree mortality and forest die-off from hotter drought in the Anthropocene. *Ecosphere*, **6**, 1–55.

Allen C.D., Macalady A.K., Chenchouni H., Bachelet D., McDowell N., Vennetier M., Kitzberger T., Rigling A., Breshears D.D., Hogg E.H., Gonzalez P., Fensham R., Zhang Z., Castro J., Demidova N., Lim J.-H., Allard G., Running S.W., Semerci A., Cobb N. (2010) A global overview of drought and heat-induced tree mortality reveals emerging climate change risks for forests. *Forest Ecology and Management*, **259**, 660–684.

Anderegg W.R.L., Klein T., Bartlett M., Sack L., Pellegrini A.F.A., Choat B., Jansen S. (2016) Meta-analysis reveals that hydraulic traits explain cross-species patterns of drought-induced tree mortality across the globe. *Proceedings of the National Academy of Sciences of the United States of America*, **113**, 5024–5029.

Blackman C.J., Creek D., Maier C., Aspinwall M.J., Drake J.E., Pfautsch S., O'Grady A., Delzon S., Medlyn B.E., Tissue D.T., Choat B. (2019) Drought response strategies and hydraulic traits contribute to mechanistic understanding of plant dry-down to hydraulic failure. *Tree Physiology*, **39**, 910–924.

Blackman C.J., Gleason S.M., Chang Y., Cook A.M., Laws C., Westoby M. (2014) Leaf hydraulic vulnerability to drought is linked to site water availability across a broad range of species and climates. *Annals of Botany*, **114**, 435–440.

Bland M.J., Altman D.G. (1986) Statistical methods for assessing agreement between two methods of clinical measurement. *The Lancet*, **327**, 307–310.

Bolker B.M. (2008) *Ecological models and data in R*. Princeton University Press, Princeton, NJ, USA.

Brando P.M., Paolucci L., Ummenhofer C.C., Ordway E.M., Hartmann H., Cattau M.E., Rattis L., Medjibe V., Coe M.T., Balch J. (2019) Droughts, wildfires, and Forest carbon cycling: a pantropical synthesis. *Annual Review of Earth and Planetary Sciences*, **47**, 555–581.

Brodersen C.R., McElrone A.J., Choat B., Matthews M.A., Shackel K.A. (2010) The dynamics of embolism repair in xylem: in vivo visualizations using high-resolution computed tomography. *Plant Physiology*, **154**, 1088–1095.

Brodribb T.J., Carriqui M., Delzon S., Lucani C. (2017) Optical measurement of stem xylem vulnerability. *Plant Physiology*, **174**, 2054–2061.

Brodribb T.J., Cochard H. (2009) Hydraulic failure defines the recovery and point of death in water-stressed conifers. *Plant Physiology*, **149**, 575–584.

Brodribb T.J., Powers J., Cochard H., Choat B. (2020) Hanging by a thread? Forests and drought. *Science*, **368**, 261–266.

Brodribb T.J., Skelton R.P., McAdam S.A.M., Bienaimé D., Lucani C.J., Marmottant P. (2016) Visual quantification of embolism reveals leaf vulnerability to hydraulic failure. *New Phytologist*, **209**, 1403–1409.

Brooks M.E., Kristensen K., van Benthem K.J., Magnusson A., Berg C.W., Nielsen A., Skaug H.J., Maechler M., Bolker B.M. (2017) glmmTMB balances speed and flexibility among packages for zero-inflated generalized linear mixed modeling. *The R Journal*, **9**, 378–400.

Brum M., Pereira L., Ribeiro R.V., Jansen S., Bittencourt P.R.L., Oliveira R.S., Saleska S.R. (2023) Reconciling discrepancies in measurements of vulnerability to xylem embolism with the pneumatic method. *New Phytologist*, **237**, 374–383.

Burlett R., Parise C., Capdeville G., Cochard H., Lamarque L.J., King A., Delzon S. (2022) Measuring xylem hydraulic vulnerability for long-vessel species: an improved methodology with the flow centrifugation technique. *Annals of Forest Science*, **79**, 5.

Carstensen B. (2004) Comparing and predicting between several methods of measurement. *Biostatistics*, **5**, 399–413.

Chen Y., Maenpuen P., Zhang Y., Barai K., Katabuchi M., Gao H., Kaewkamol S., Tao L., Zhang J. (2021) Quantifying vulnerability to embolism in tropical trees and lianas using five methods: can discrepancies be explained by xylem structural traits? *New Phytologist*, **229**, 805–819.

Choat B., Brodribb T.J., Brodersen C.R., Duursma R.A., López R., Medlyn B.E. (2018) Triggers of tree mortality under drought. *Nature*, **558**, 531–539.

Choat B., Drayton W.M., Brodersen C., Matthews M.A., Shackel K.A., Wada H., Mcelrone A.J. (2010) Measurement of vulnerability to water stress-induced cavitation in grapevine: a comparison of four techniques applied to a long-vesseled species: comparison of vulnerability curve technique in grapevine. *Plant, Cell & Environment*, **33**, 1502–1512.

Cochard H., Badel E., Herbette S., Delzon S., Choat B., Jansen S. (2013) Methods for measuring plant vulnerability to cavitation: a critical review. *Journal of Experimental Botany*, **64**, 4779–4791.

Cochard H., Cruiziat P., Tyree M.T. (1992) Use of positive pressures to establish vulnerability curves: further support for the air-seeding hypothesis and implications for pressure-volume analysis. *Plant Physiology*, **100**, 205–209.

Cochard H., Damour G., Bodet C., Tharwat I., Poirier M., Améglio T. (2005) Evaluation of a new centrifuge technique for rapid generation of xylem vulnerability curves. *Physiologia Plantarum*, **124**, 410–418.

Cochard H., Herbette S., Barigah T., Badel E., Ennajeh M., Vilagrosa A. (2010) Does sample length influence the shape of xylem embolism vulnerability curves? A test with the Cavitron spinning technique: shape of xylem embolism vulnerability curves. *Plant, Cell & Environment*, **33**, 1543–1552.

Cramér H. (1928) On the composition of elementary errors. II Statistical applications. *Skandinavisk Aktuarietidskrift*, **11**, 141–180.

De Baerdemaeker N.J.F., Arachchige K.N.R., Zinkernagel J., Van den Bulcke J., Van Acker J., Schenk H.J., Steppe K. (2019) The stability enigma of hydraulic vulnerability curves: addressing the link between hydraulic conductivity and drought-induced embolism. *Tree Physiology*, **39**, 1646–1664.

de V Barros F., Bittencourt P.R.L., Brum M., Restrepo-Coupe N., Pereira L., Teodoro G.S., Saleska S.R., Borma L.S., Christoffersen B.O., Penha D., Alves L.F., Lima A.J.N., Carneiro V.M.C., Gentine P., Lee J.-E., Aragão L.E.O.C., Ivanov V., Leal L.S.M., Araujo A.C., Oliveira R.S. (2019) Hydraulic traits explain differential responses of Amazonian forests to the 2015 El Niño-induced drought. *New Phytologist*, **223**, 1253–1266.

Delzon S., Cochard H. (2014) Recent advances in tree hydraulics highlight the ecological significance of the hydraulic safety margin. *New Phytologist*, **203**, 355–358.

Field C.B., Barros V., Stocker T.F., Dahe Q. (Eds) (2012) *Managing the risks of extreme events and disasters to advance climate change adaptation: special report of the intergovernmental panel on climate change*. Cambridge University Press, Cambridge, UK. Available from https://www.cambridge.org/core/books/managing-the-risks-of-extreme-events-and-disasters-to-advance-climate-change-adapta

tion/0D6C7E5AAD12D00CB305C9933422989C (accessed 16 July 2020).

Franz G., Kram G. (1985) Structural investigations on the watersoluble polysaccharides of lime tree flowers. *Die Pharmazie*, **41**, 501.

Gillner S., Korn S., Hofmann M., Roloff A. (2017) Contrasting strategies for tree species to cope with heat and dry conditions at urban sites. *Urban Ecosystem*, **20**, 853–865.

Guan X., Pereira L., McAdam S.A.M., Cao K.-F., Jansen S. (2021) No gas source, no problem: proximity to pre-existing embolism and segmentation affect embolism spreading in angiosperm xylem by gas diffusion. *Plant, Cell & Environment*, **44**, 1329–1345.

Hacke U.G., Venturas M.D., MacKinnon E.D., Jacobsen A.L., Sperry J.S., Pratt R.B. (2015) The standard centrifuge method accurately measures vulnerability curves of long-vesselled olive stems. *New Phytologist*, **205**, 116–127.

Hajek P., Link R.M., Nock C.A., Bauhus J., Gebauer T., Gessler A., Kovach K., Messier C., Paquette A., Saurer M., Scherer-Lorenzen M., Rose L., Schuldt B. (2022) Mutually inclusive mechanisms of drought-induced tree mortality. *Global Change Biology*, **28**, 3365–3378.

Hartmann H., Link R.M., Schuldt B. (2021) A whole-plant perspective of isohydry: stem-level support for leaf-level plant water regulation. *Tree Physiology*, **41**, 901–905.

Hochberg U., Windt C.W., Ponomarenko A., Zhang Y.-J., Gersony J., Rockwell F.E., Holbrook N.M. (2017) Stomatal closure, basal leaf embolism, and shedding protect the hydraulic integrity of grape stems. *Plant Physiology*, **174**, 764–775.

Isasa E., Link R.M., Jansen S., Tezeh F.R., Kaack L., Sarmento C.J., Schuldt B. (2023) Addressing controversies in the xylem embolism resistance–vessel diameter relationship. *New Phytologist*, **238**, 283–296.

Jansen S., Guan X., Kaack L., Trabi C., Miranda M.T., Ribeiro R.V., Pereira L. (2020) The Pneumatron estimates xylem embolism resistance in angiosperms based on gas diffusion kinetics: a mini-review. ISHS Acta Horticulturae 1300: 193–200.

Jansen S., Schuldt B., Choat B. (2015) Current controversies and challenges in applying plant hydraulic techniques. *New Phytologist*, **205**, 961–964.

Kiorapostolou N., Galiano-Pérez L., von Arx G., Gessler A., Petit G. (2018) Structural and anatomical responses of *Pinus sylvestris* and *Tilia platyphyllos* seedlings exposed to water shortage. *Trees*, **32**, 1211–1218.

Klepsch M., Zhang Y., Kotowska M.M., Lamarque L.J., Nolf M., Schuldt B., Torres-Ruiz J.M., Qin D.-W., Choat B., Delzon S., Scoffoni C., Cao K.-F., Jansen S. (2018) Is xylem of angiosperm leaves less resistant to embolism than branches? Insights from microCT, hydraulics, and anatomy. *Journal of Experimental Botany*, **69**, 5611–5623.

Lande R., Engen S., Saether B.-E. (2003) *Stochastic population dynamics in ecology and conservation*. Oxford University Press, Oxford, UK.

Leuschner C., Wedde P., Lübbe T. (2019) The relation between pressure–volume curve traits and stomatal regulation of water potential in five temperate broadleaf tree species. *Annals of Forest Science*, **76**, 60.

Li X., Xi B., Wu X., Choat B., Feng J., Jiang M., Tissue D. (2022) Unlocking drought-induced tree mortality: physiological mechanisms to modeling. *Frontiers in Plant Science*, **13**, 835921. (accessed 6 April 2022. https://www.frontiersin.org/article/10.3389/fpls.2022.835921

Li Y., Sperry J.S., Taneda H., Bush S.E., Hacke U.G. (2008) Evaluation of centrifugal methods for measuring xylem cavitation in conifers, diffuse- and ring-porous angiosperms. *New Phytologist*, **177**, 558–568.

Link R.M., Schuldt B., Choat B., Jansen S., Cobb A.R. (2018) Maximum-likelihood estimation of xylem vessel length distributions. *Journal of Theoretical Biology*, **455**, 329–341.

López R., Nolf M., Duursma R.A., Badel E., Flavel R.J., Cochard H., Choat B. (2019) Mitigating the open vessel artefact in centrifuge-based measurement of embolism resistance. *Tree Physiology*, **39**, 143–155.

Martin-StPaul N., Delzon S., Cochard H. (2017) Plant resistance to drought depends on timely stomatal closure. *Ecology Letters*, **20**, 1437–1447.

Martin-StPaul N.K., Longepierre D., Huc R., Delzon S., Burlett R., Joffre R., Rambal S., Cochard H. (2014) How reliable are methods to assess xylem vulnerability to cavitation? The issue of "open vessel" artifact in oaks. *Tree Physiology*, **34**, 894–905.

McDowell N.G., Fisher R.A., Xu C., Domec J.C., Hölttä T., Mackay D.S., Sperry J.S., Boutz A., Dickman L., Gehres N., Limousin J.M., Macalady A., Martínez-Vilalta J., Mencuccini M., Plaut J.A., Ogée J., Pangle R.E., Rasse D.P., Ryan M.G., Sevanto S., Waring R.H., Williams A.P., Yepez E.A., Pockman W.T. (2013a) Evaluating theories of drought-induced vegetation mortality using a multimodel-experiment framework. *New Phytologist*, **200**, 304–321.

McDowell N.G., Ryan M.G., Zeppel M.J.B., Tissue D.T. (2013b) Feature: improving our knowledge of drought-induced forest mortality through experiments, observations, and modeling. *New Phytologist*, **200**, 289–293.

Meinzer F.C., Johnson D.M., Lachenbruch B., McCulloh K.A., Woodruff D.R. (2009) Xylem hydraulic safety margins in woody plants: coordination of stomatal control of xylem tension with hydraulic capacitance. *Functional Ecology*, **23**, 922–930.

Moser A., Rötzer T., Pauleit S., Pretzsch H. (2016) The urban environment can modify drought stress of small-leaved lime (*Tilia cordata* mill.) and black locust (*Robinia pseudoacacia* L.). *Forests*, **7**, 71.

Nolf M., Lopez R., Peters J.M.R., Flavel R.J., Koloadin L.S., Young I.M., Choat B. (2017) Visualization of xylem embolism by X-ray microtomography: a direct test against hydraulic measurements. *New Phytologist*, **214**, 890–898.

Ogle K., Barber J.J., Willson C., Thompson B. (2009) Hierarchical statistical modeling of xylem vulnerability to cavitation. *New Phytologist*, **182**, 541–554.

Oliveira R.S., Costa F.R.C., van Baalen E., de Jonge A., Bittencourt P.R., Almanza Y., de V Barros F., Cordoba E.C., Fagundes M.V., Garcia S., Guimaraes Z.T.M., Hertel M., Schietti J., Rodrigues-Souza J., Poorter L. (2019) Embolism resistance drives the distribution of Amazonian rainforest tree species along hydro-topographic gradients. *New Phytologist*, **221**, 1457–1465.

Pammenter N.W., Van der Willigen C. (1998) A mathematical and statistical analysis of the curves illustrating vulnerability of xylem to cavitation. *Tree Physiology*, **18**, 589–593.

Pereira L., Bittencourt P.R.L., Oliveira R.S., Junior M.B.M., Barros F.V., Ribeiro R.V., Mazzafera P. (2016) Plant pneumatics: stem air flow is related to embolism – New perspectives on methods in plant hydraulics. *New Phytologist*, **211**, 357–370.

Pereira L., Bittencourt P.R.L., Pacheco V.S., Miranda M.T., Zhang Y., Oliveira R.S., Groenendijk P., Machado E.C., Tyree M.T., Jansen S., Rowland L., Ribeiro R.V. (2020a) The Pneumatron: an automated pneumatic apparatus for estimating xylem vulnerability to embolism at high temporal resolution. *Plant, Cell & Environment*, **43**, 131–142.

Pereira L., Bittencourt P.R.L., Rowland L., Brum M., Miranda M.T., Pacheco V.S., Oliveira R.S., Machado E.C., Jansen S., Ribeiro R.V. (2021) Using the pneumatic method to estimate embolism resistance in species with long vessels: a commentary on the article "A comparison of five methods to assess embolism resistance in trees". *Forest Ecology and Management*, **479**, 118547.

Pereira L., Miranda M.T., Pires G.S., Pacheco V.S., Guan X., Kaack L., Karimi Z., Machado E.C., Jansen S., Tyree M.T., Ribeiro R.V. (2020b) A semi-automated method for measuring xylem vessel length distribution. *Theoretical and Experimental Plant Physiology*, **32**, 331–340.

Pigott D. (2012) *Lime-trees and basswoods: a biological monograph of the genus Tilia*. Cambridge University Press, Cambridge, UK.

Pivovaroff A.L., Sack L., Santiago L.S. (2014) Coordination of stem and leaf hydraulic conductance in southern California shrubs: a test of the hydraulic segmentation hypothesis. *New Phytologist*, **203**, 842–850.

Pratt R.B., Castro V., Fickle J.C., Jacobsen A.L. (2020) Embolism resistance of different aged stems of a California oak species (*Quercus douglasii*): optical and microCT methods differ from the benchtop-dehydration standard. *Tree Physiology*, **40**, 5–18.

Pya N., Wood S.N. (2015) Shape constrained additive models. *Statistics and Computing*, **25**, 543–559.

R Core Team (2020) *R: a language and environment for statistical computing*. R Foundation for Statistical Computing, Vienna, Austria. Available from https://www.R-project.org/

Rodriguez-Dominguez C.M., Forner A., Martorell S., Choat B., Lopez R., Peters J.M.R., Pfautsch S., Mayr S., Carins-Murphy M.R., McAdam S.A.M., Richardson F., Diaz-Espejo A., Hernandez-Santana V., Menezes-Silva P.E., Torres-Ruiz J.M., Batz T.A., Sack L. (2022) Leaf water potential measurements using the pressure chamber: synthetic testing of assumptions towards best practices for precision and accuracy. *Plant, Cell & Environment*, **45**, 2037–2061.

Rosner S., Heinze B., Savi T., Dalla-Salda G. (2019) Prediction of hydraulic conductivity loss from relative water loss: new insights into water storage of tree stems and branches. *Physiologia Plantarum*, **165**, 843–854.

Sergent A.S., Varela S.A., Barigah T.S., Badel E., Cochard H., Dalla-Salda G., Delzon S., Fernández M.E., Guillemot J., Gyenge J., Lamarque L.J., Martinez-Meier A., Rozenberg P., Torres-Ruiz J.M., Martin-StPaul N.K. (2020) A comparison of five methods to assess embolism resistance in trees. *Forest Ecology and Management*, **468**, 118175.

Sorz J., Hietz P. (2006) Gas diffusion through wood: implications for oxygen supply. *Trees*, **20**, 34–41.

Sperry J.S., Donnelly J.R., Tyree M.T. (1988) A method for measuring hydraulic conductivity and embolism in xylem. *Plant, Cell and Environment*, **11**, 35–40.

Torres-Ruiz J.M., Cochard H., Mayr S., Beikircher B., Diaz-Espejo A., Rodriguez-Dominguez C.M., Badel E., Fernández J.E. (2014) Vulnerability to cavitation in *Olea europaea* current-year shoots: further

evidence of an open-vessel artifact associated with centrifuge and air-injection techniques. *Physiologia Plantarum*, **152**, 465–474.

Torres-Ruiz J.M., Jansen S., Choat B., McElrone A.J., Cochard H., Brodribb T.J., Badel E., Burlett R., Bouche P.S., Brodersen C.R., Li S., Morris H., Delzon S. (2015) Direct X-ray microtomography observation confirms the induction of embolism upon xylem cutting under tension. *Plant Physiology*, **167**, 40–43.

Trenberth K.E., Dai A., van der Schrier G., Jones P.D., Barichivich J., Briffa K.R., Sheffield J. (2014) Global warming and changes in drought. *Nature Climate Change*, **4**, 17–22.

Trueba S., Pouteau R., Lens F., Feild T.S., Isnard S., Olson M.E., Delzon S. (2017) Vulnerability to xylem embolism as a major correlate of the environmental distribution of rain forest species on a tropical Island. *Plant, Cell & Environment*, **40**, 277–289.

Urli M., Porte A.J., Cochard H., Guengant Y., Burlett R., Delzon S. (2013) Xylem embolism threshold for catastrophic hydraulic failure in angiosperm trees. *Tree Physiology*, **33**, 672–683.

Venturas M.D., Pratt R.B., Jacobsen A.L., Castro V., Fickle J.C., Hacke U.G. (2019) Direct comparison of four methods to construct xylem vulnerability curves: differences among techniques are linked to vessel network characteristics. *Plant, Cell & Environment*, **42**, 2422–2436.

Wang Y., Liu J., Tyree M.T. (2015) Stem Hydraulic Conductivity depends on the pressure at which it is measured and how this dependence can be used to assess the tempo of bubble pressurization in recently cavitated vessels. *Plant Physiology*, **169**, 2597–2607.

Wheeler J.K., Huggett B.A., Tofte A.N., Rockwell F.E., Holbrook N.M. (2013) Cutting xylem under tension or supersaturated with gas can generate PLC and the appearance of rapid recovery from embolism: sampling-induced embolism. *Plant, Cell & Environment*, **36**, 1938–1949.

Wickham H., Averick M., Bryan J., Chang W., McGowan L.D., François R., Grolemund G., Hayes A., Henry L., Hester J., Kuhn M., Pedersen T.L., Miller E., Bache S.M., Müller K., Ooms J., Robinson D., Seidel D.P., Spinu V., Takahashi K., Vaughan D., Wilke C., Woo K., Yutani H. (2019) Welcome to the tidyverse. *Journal of Open Source Software*, **4**, 1686.

Wolfe B.T., Sperry J.S., Kursar T.A. (2016) Does leaf shedding protect stems from cavitation during seasonal droughts? A test of the hydraulic fuse hypothesis. *New Phytologist*, **212**, 1007–1018.

Wu M., Zhang Y., Oya T., Marcati C.R., Pereira L., Jansen S. (2020) Root xylem in three woody angiosperm species is not more vulnerable to embolism than stem xylem. *Plant and Soil*, **450**, 479–495.

Yang D., Pereira L., Peng G., Ribeiro R.V., Kaack L., Jansen S., Tyree M.T. (2023) A unit pipe pneumatic model to simulate gas kinetics during measurements of embolism in excised angiosperm xylem. *Tree Physiology*, **43**, 88–101.

Zhang Y., Lamarque L.J., Torres-Ruiz J.M., Schuldt B., Karimi Z., Li S., Qin D.-W., Bittencourt P., Burlett R., Cao K.-F., Delzon S., Oliveira R., Pereira L., Jansen S. (2018) Testing the plant pneumatic method to estimate xylem embolism resistance in stems of temperate trees. *Tree Physiology*, **38**, 1016–1025.

Zhao H., Jiang Z., Ma J., Cai J. (2020) What causes the differences in cavitation resistance of two shrubs? Wood anatomical explanations and reliability testing of vulnerability curves. *Physiologia Plantarum*, **169**, 156–168.

Zhao H., Li Y., Liao S., Jiang Z., Cai J. (2023) Further test of pneumatic method in constructing vulnerability curves using six tree species with contrasting xylem anatomy. *Forests*, **14**, 293.

Zhu S.-D., Liu H., Xu Q.-Y., Cao K.-F., Ye Q. (2016) Are leaves more vulnerable to cavitation than branches? *Functional Ecology*, **30**, 1740–1744.